

# Impact of Wetting Film Flow in Pore Scale Displacement

E. Unsal\* and Emmanuel Moulet-Vargas

TOTAL Geoscience Research Centre, Aberdeen, UK

*This paper was prepared for presentation at the International Symposium of the Society of Core Analysts held in Napa Valley, California, USA, 16-19 September, 2013*

## ABSTRACT

In flow through porous media, the wetting films may contribute many phenomena which directly affect the oil recovery. While some of these phenomena might limit the overall recovery process tremendously by trapping the non-wetting phase, the others may provide means for certain molecular processes to occur. The latter has gained importance over the last few decades and led some of the enhanced oil recovery processes (EOR) to develop. Whether limiting or enhancing the recovery these films have an important impact in scales larger than their own. Due to their very thin structure (a few micrometers the most) experiments often get limited, and direct observation is not possible, especially in a three-dimensional porous medium. The numerical simulations also struggle with such small scales as it requires a very high resolution to capture the film flow physics and a significant computational power is necessary to simulate flow on a sample with a representative size within a reasonable time.

We present a summary on the wetting film flow and try to put them in perspective regarding in which scale they occur and in what scale(s) their impacts are visible and unavoidable. First a few experiments outline when/how the films form and provide visual proof on their behavior during multi-phase flow. The findings of these experiments clearly show the impact of, for example, snap-off events which provide an important basis for the numerical methods. We then present a dynamic pore network model (PNM) which accommodates the wetting film flow, coupled into the flow in network elements without any sub-gridding. For both wetting and non-wetting phase, the flow equation is solved and the wetting phase pressures calculated in the wetting films as well as each network element. This way of coupling helps to upscale a nano/micro scale event to the Darcy scale. But, regardless of the physics a PNM has, its prediction capacity is always dependent on the quality of the network extraction process. Direct methods, free from the extraction ambiguities, can provide a much more detailed physical representation of the processes, but at a higher computational cost. Here, these two numerical approaches are also compared in terms of their capability and way of handling the thin film flow, their potential to simulate EOR processes and the computational efficiency.

## INTRODUCTION

For the simulation of multiphase flow in porous rock an accurate description of pore scale displacement processes has recently gained more importance in particular in the context

of EOR. However, the multiscale nature of pore sizes in reservoir rock [1-4] and displacement processes indicated in Figure 1 poses a substantial challenge for numerical simulators and also experimentation. There are various physical processes at different length scales with impact on the macroscale (= Darcy scale) displacement ranging from few nanometers to centimeters.

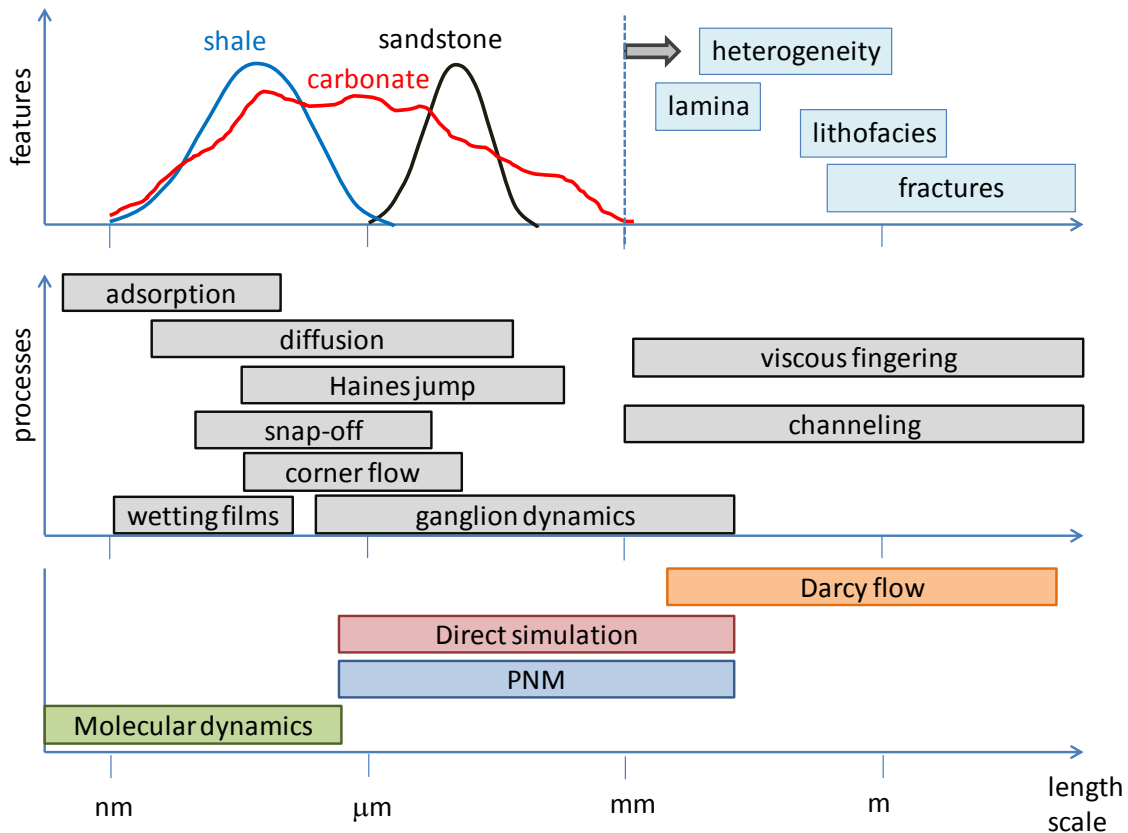


Figure 1: Pore sizes of rock/fluids (top), length scales associated with processes in multiphase flow simulation (middle), and simulation approaches for multiphase flow (bottom).

In many cases the actual processes occurring in rock are not well understood. Direct observation is not always possible as current experimental technology is limited; the numerical methods can provide some insight. A ‘one for all scales’ approach does not currently exist and is also not in sight. Therefore a selection of the most appropriate method should be made based on the criteria such as the scale in which the problem originates and starts creating impact on the consecutive larger scales. Each method spans a certain range in which phenomena or features are explicitly resolved. Direct methods that are based on a discretization of the pore space aim to cover a representative elementary volume (REV) typically use grid block sizes of few hundred nanometers, i.e. orders of magnitude larger than the molecular scale on which properties like wettability or surface tension is controlled. These sub-resolution features are then implemented using

effective medium properties like contact angle and interfacial tension which are also experimentally accessible. Other methods like PNMs are also constrained by the same resolution as the direct approach. However, they can span over a wider range of length scales because the pore scale displacement is decomposed into a set of elementary processes like thin wetting film flow (*nm* scale) which are then *represented* using, numerically, very effective rule-based approach. They don't require an additional, high resolution sub-grid which may not be always possible.

In the following sections we focus on the modelling of imbibition processes which are of particular interest for the recovery of oil and gas. In imbibition, snap-off disconnects the non-wetting phase (typically oil or gas) which leads to trapping and irreducible oil saturation reducing the recovery efficiency. In these snap-off processes, the advancement of the wetting phase in thin film and corner flow plays a key role. These wetting films are known to have thicknesses in orders of *nm* to  $\mu m$  [5] (Figure 1). What is less known is at what size they can provide sufficient connectivity and affect the overall wetting phase flow. To study such films a numerical method which represents the relevant physics in the corresponding scale is required. Dynamic PNMs, for instance, have "infinite resolution" for processes like thin film and corner flow but the question is whether displacement rules are correct and the delicate balance of capillary and viscous processes are correctly captured. Moreover these models are highly dependent on the quality of the extraction process. For many direct methods, the extraction process is irrelevant and they are not based on such balance rules. But the thin film flow may require further sub-resolution, while the corner flow might be explicitly resolved.

Here, a dynamic PNM for imbibition is presented. First the model is analysed based on its capability of handling the wetting film flow and snap-off during counter-current imbibition. Then a comparative study is presented using a direct Navier-Stokes flow approach with respect to the handling of film flow. Lastly the relevance of film flow in EOR applications is discussed, followed by a demonstration in which the PNM is coupled with the geochemical software PHREEQC. This coupling extends the EOR capabilities of PNM by allowing chemical interactions between the fluid and rock surface during flow. Any adsorption and diffusion of a wettability altering agent affect local contact angle and interfacial tension, consequently local capillary pressures and overall flow behavior.

## **WETTING FILMS AND SNAP-OFF**

In strongly water-wet rock space, the water phase wets the rock surface forming thin wetting films in angular cavities providing full wetting phase connectivity, even at very low saturations. Due to this connectivity, during imbibition, the injected wetting phase is able to flow throughout the pore space via the wetting films ahead of the advancing meniscus. While flowing, the wetting films may bridge across the waists of the pores at various places 'within the pore space' and snap-off due to pore-scale capillary instability (Figure 2a). This may result in trapped non-wetting phase as shown in the micromodel experiment in (Figure 2b). This mechanism is believed to be the main cause of hysteresis

and entrapment. The effect is more significant if the flow regime is more capillary dominated, i.e., highly-wetting, low injection rates.

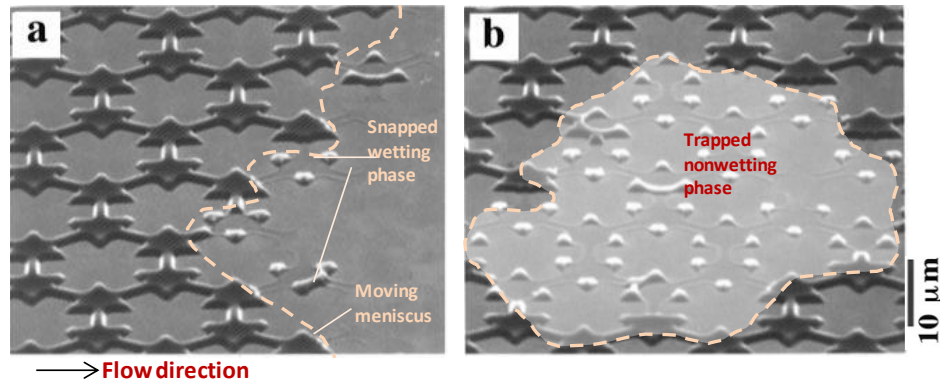


Figure 2: (a) Wetting film snap-off ahead of advancing meniscus ‘within the pore space’. The model is saturated with nonwetting-phase (same color as the micromodel), and the wetting phase is injected from left (black). A few film snap-off is observed slightly ahead of the moving meniscus [6], (b) Further into the experiments, a high number of wetting film snap-offs result in trapped non-wetting phase.

Snap-off occurring ‘within the pore space’ can immobilize and trap large amounts of nonwetting-phase, but snap-off ‘at the open surface of the pore space’ causes the *recovering* nonwetting-phase break into small mobile blobs (nonwetting phase bubbles). The two phenomena are different but related as the corner films play an important role in both. The underlying principle in the latter is that for a fixed volume, a sphere has less surface area than a cylinder. For a perfectly wetting liquid lining the walls of a cylindrical tube, the interface curvature is  $1/R$  (where  $R$  is the tube radius), whereas if the same volume of fluid is a slug spanning the tube, the curvature is  $2/R$  and the latter has less surface energy and so is more stable. One of the main implication of such snap-off is the constantly changing outlet boundary pressure due to the changing bubble size. The effect is also periodic because bubbles form consecutively.

The essence of this mechanism was studied in detail in a previous model experiment where bubble snap-off during counter-current spontaneous imbibition was investigated [7]. Three laterally interconnected capillaries of different sizes are connected to the wetting-phase (oil) reservoir at one end (see Figure 3); the other side is closed to flow. The wetting phase imbibes into each capillary, but advances further only into the two smaller ones. This compresses the non-wetting phase (air), consequently the pressure increases causing displacement at the meniscus location with the lowest capillary entry pressure, i.e. the largest capillary and in the direction backwards into the wetting-phase reservoir. Once the air-oil interface reaches to the end of capillary, a bubble starts to form. As the air bubble grows into the reservoir its curvature changes which results a visible drop in the back pressure in the non-wetting phase. But this growth eventually comes to an end due to surface instability causing the bubble to snap off. The pressure

recovers up to its original value again. The pressure recordings clearly show the bubble formation and the snap-off point (Figure 3d).

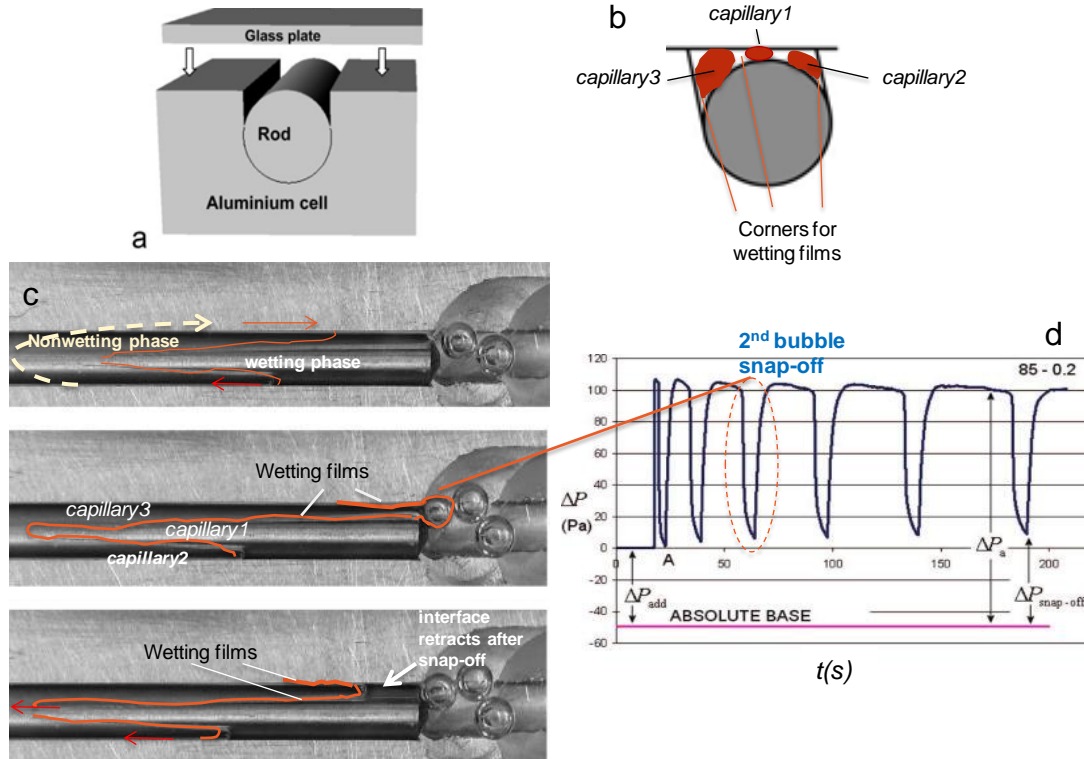


Figure 3: Spontaneous counter-current imbibition experimental set-up [7], (a-b) capillary cross-sections, (c) view from top: the capillaries are open to the reservoir on the right. Left side is closed to flow; here a pressure transducer is connected and measures the oil pressure, (d) Nonwetting phase bubble formation and snap-off in the oil reservoir.

## NUMERICAL MODELING OF SNAP-OFF EVENTS

### Pore Network Models (PNMs)

In pore network models the geometry of the pore space is abstracted into simple geometrical shapes like spheres, cubes and cylinders typically, with angular cross sections. The number and coordination of these structures are completely dependent on the extraction process, which introduces a lot of ambiguity to the network geometry as various extraction algorithms may predict entirely different networks. On the more positive side, for these simplified shapes the hydraulic conductivities can be analytically approximated over a large saturation range which has the advantage that no sub-gridding of pores or throats is required. However certain variants of PNMs do sub-discretize pores into centers and corners [8]. The wetting films may exist throughout the whole network

and they can be very thin ( $\ll 1\mu m$ ) [5]. Instead of any fine gridding, these films are coupled into the flow equations, i.e., each element of the network is assigned a film flow. This way PNM's have "infinite" resolution for wetting films while solving flow equations in Darcy scale (Figure 1) performing an efficient upscaling process. In a grid based approach this would require a very fine grid size.

In dynamic PNM's, which is the case here, the balance of viscous and capillary forces is considered by solving explicitly the phase pressures including the viscous pressure drop in each element and the wetting films [8, 9]. The outlet boundary condition is, however, significantly different. It is often assumed that the displacement happens in a co-current manner, and both phases flow in the same direction from inlet towards the outlet. The displaced phase is assumed to be connected to a relatively large reservoir of the same phase at the exit, which generates a fixed (or no) resistance for the displaced phase to leave the pore network. Here, the intention is to model a counter-current displacement; only one face of the network is open to flow and it is connected to a reservoir filled with the injected fluid (wetting) only. In order to exit the pore network the displaced nonwetting phase has to overcome a much greater resistance, which will result in the nonwetting phase breaking into small bubbles at the open face of the pore space. Moreover because the size of the nonwetting phase bubble is continuously changing during the displacement, a varying pressure (equal to capillary pressure of the bubble) is generated as an outlet boundary condition. The wetting phase, on the other hand, is fully connected via the wetting films; therefore there is no pressure for it to flow out the pore space.

The experiment in Figure 3, the injected oil phase (wetting) has higher viscosity compared to the displaced air phase. Air cannot generate a high viscous resistance to flow and it is compressible. But would that be the case if the displaced fluid was more viscous compared to the injected phase? If the same experimental set up is used for a two-phase fluid system where the viscosities are similar, it would take perhaps significantly longer as the displaced phase resist to flow due to its comparable viscosity to the injected phase. In order to study the viscosity ratio effect (mobility number,  $M = \mu_{disp}/\mu_{inj}$ ) during counter-current imbibition, three different fluid systems were simulated using the set-up in Figure 3 (see Figure 4, Table 1). Three capillaries of different cross section are represented by three rows of pores of different size which are interconnected via throats (in the experiment the interconnection is continuous). The pore and throat elements have square cross-sections with an inscribed radius shown in Figure 4 (far right). Each element is assigned with thin films in its angular corners with a thickness of 0.001 times of its inscribed radius. The network is open to flow only on the left side; the remaining three sides are no-flow boundaries. The pore space is initially filled with the non-wetting phase (oil, green), and it is connected to the wetting water phase (blue) which enters from the left. Both fluids are assumed to be incompressible and only the final steps of the simulations are shown. Maximum bubble radius is assumed to be 1.5 times of the capillary (I) radius where it is emerging from. The bubble growth is tracked as the

nonwetting phase flows out of the network and when its radius reaches the maximum value, it snaps off.

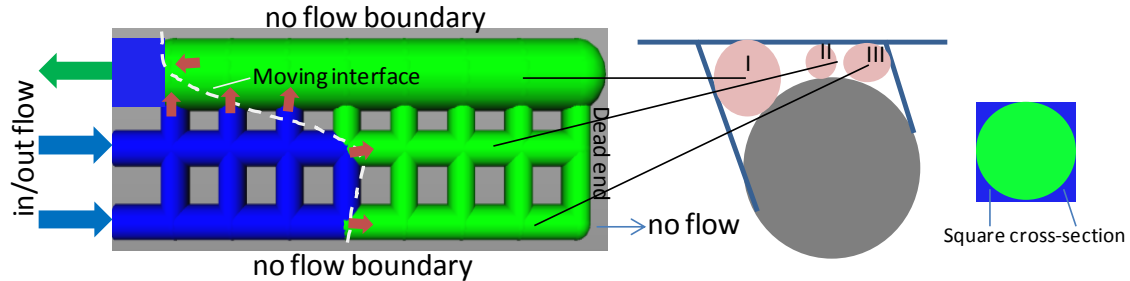


Figure 4: Network model for counter-current imbibition; in/outflow are possible only via left side. Green is the non-wetting and blue is the wetting phase. The advancing interface is indicated with white dashed line. The red arrows indicate where the possible moves are along the interface. The radii of the capillaries are: largest (I) 100 $\mu\text{m}$ , smallest (II) 45  $\mu\text{m}$  and medium (III) 50  $\mu\text{m}$ . The pore/throats have square cross-sections in the PNM.

Table 1. Fluid system parameters.

Case	$\mu_{inj}$ (Pas)	$\mu_{displaced}$ (Pas)	$\sigma$ (N/m)	Injection rate ( $\text{m}^3\text{s}^{-1}$ )	Log(Ca)
I. Water-lighter oil	1E-3(water)	1E-1(oil)	0.02	1E-9	-3.4
II. Water-lighter oil	1E-3(water)	1E-1(oil)	0.02	1E-15	-9.4
III. Water-heavy oil	1E-3(water)	1 (oil)	0.02	1E-15	-9.4

In Case I the fluid system has a mobility ratio of  $M=100$  and has the highest injection rate (highest  $Ca$ ) representing a forced injection process. Consequently, the viscous forces are expected to be more significant (Figure 5a). Water is initially able imbibe into two smaller capillaries; displaced oil starts forming a bubble. As the imbibition progresses the oil pressure increases at the dead end (red zone on the right) and bubble continues to grow reducing the opposing capillary pressure at the outlet (left). The net force ( $\Delta P_{net}$ ) along the water-oil interface is a function of the local  $P_c$ , water and oil pressures ( $\Delta P_{net} = \Delta P_c - (P_o - P_w)$ ). The red arrows indicate where the next move may occur along the interface and the size of the arrow shows the strength of  $\Delta P_{net}$ . The interface moves towards where  $\Delta P_{net}$  is the highest at that particular time.

Advancing water front generates a high pressure in the oil phase on the right. The pressure gradient in the oil declines towards the open end where the bubble constantly grows and bubble  $\Delta P_c$  decreases. At some point, the  $\Delta P_{net}$  is not large enough push the oil towards left, and due to the reduced resistance at the outlet it becomes easier for water to exit via the outlet. It then cuts the oil connection from the outlet and terminates the bubble growth. After this stage the water is not able to mobilize the oil any longer, and just flows out of the inlet. The progression of the bubble is shown in Figure 6a. Perhaps water would advance further to the right if the oil wasn't assumed to be incompressible.

Case II has the identical fluids, but water is injected spontaneously; the system is capillary dominated (Figure 5b). The  $P_c$  effect is much greater in  $\Delta P_{net}$ . The pressure in the water phase is lower, and not enough to mobilize the heavier oil. After only a couple of steps, the interface faces a lower resistance at the outlet and flows out via the outlet by trapping the oil. The pressure profile in the pore space just before the water cuts oil connectivity is shown in Figure 6b. Case III is also spontaneous imbibition with  $M = 1000$  (Figure 5c). As the viscosity contrast increases, there is hardly enough pressure to mobilize the oil. Consequently water takes a short cut via the outlet back into the reservoir. In both Case II and Case III the bubble is terminated before reaching its final size.

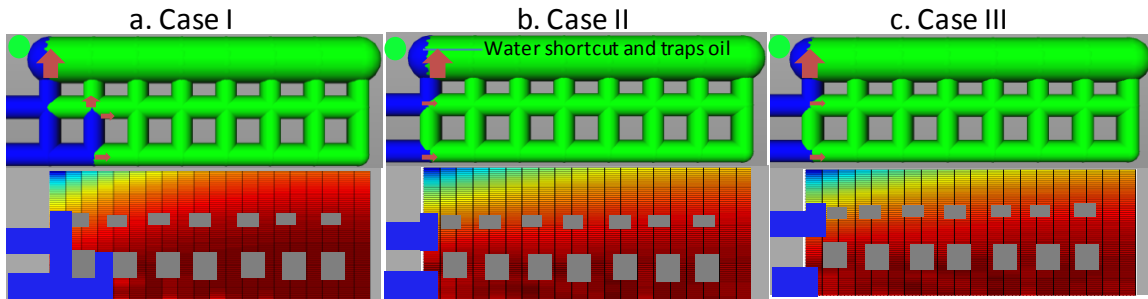


Figure 5: Displacement (top) and oil pressure (bottom) profiles in a highly water-wet systems. Oil (green) pressure gradient (min-max) in Case I=2400Pa (left)-6600Pa (most right), Case II:45Pa -245Pa, Case III:45Pa(left)-310Pa (most right).

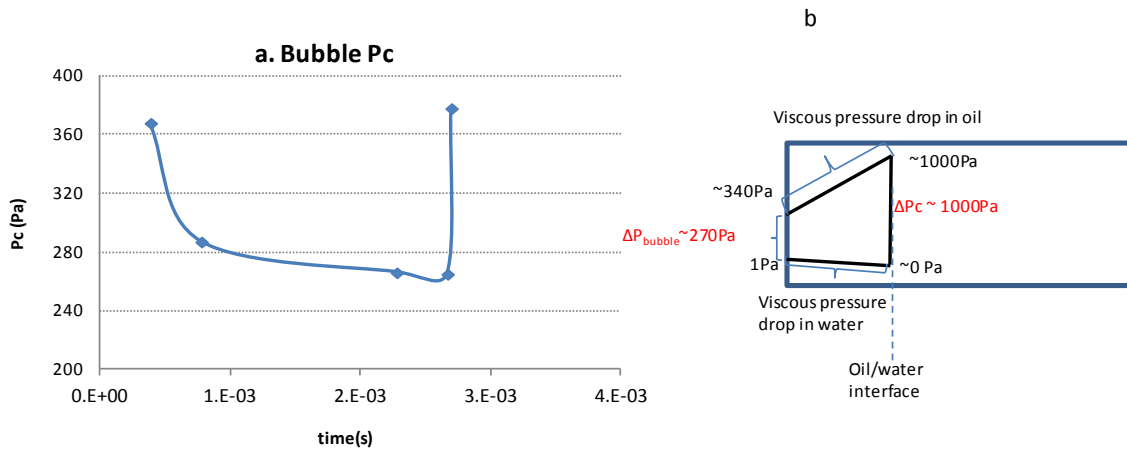


Figure 6: (a) Change in the bubble capillary pressure as it grows in Case I, (b) pressure profile at the end of the counter-current imbibition of Case II.

### Direct Methods

Direct simulation methods can be grouped into two categories: continuum mechanics based methods and particle-based methods (the latter will not be discussed further here). Direct continuum mechanics methods explicitly solve the set of continuum fluid dynamics partial differential equations (e.g. Navier-Stokes) on the real geometry of the



pore space as a boundary condition and sub-discretize/ grid each individual pore. Typical approaches use grid block sizes of 0.5-15  $\mu\text{m}$  which allows (single-phase) REV of sandstone rock at a resolution where Haines jumps [10] and corner flow can be resolved but not necessarily thin films. The main challenge is the treatment of the liquid-liquid interfaces, which typically move during the displacement and undergo topological changes during breakup and coalescence in ganglion flow. Direct Navier-Stokes approaches typically track the fluid interfaces by Level-set (LS) or Volume-of-fluid (VoF) methods. The liquid-solid boundaries are treated in an effective way using concepts like surface energy and contact angles to describe the rock-fluid interaction.

In this particular example of a direct method displayed in Figure 7 (left), initially the capillary is saturated with the nonwetting (oil, red) phase, no wetting films are present [11]. The contact angle is set to zero. As the wetting phase (water, blue) is applied from the left, the wetting films are gradually formed at the location of the interface; because for such contact angle of representing a strongly water-wet condition, it is energetically more favorable that water contacts the solid instead of oil. The actual snap-off process traps the fraction of oil according to the temporal evolution of the pressure field. On the right of Figure 7 the PNM representation of the event is shown: with the PNM the wetting films have to pre-exist and snap-off occurs at a pre-defined threshold value of the capillary pressure which is the phase pressure difference between the thin water film and the oil in the element representing the throat. Often it is not possible to calculate a detailed pressure distribution of the phases in each element with PNM. Pressure is usually known at the center points or at the few discretized point of each element.

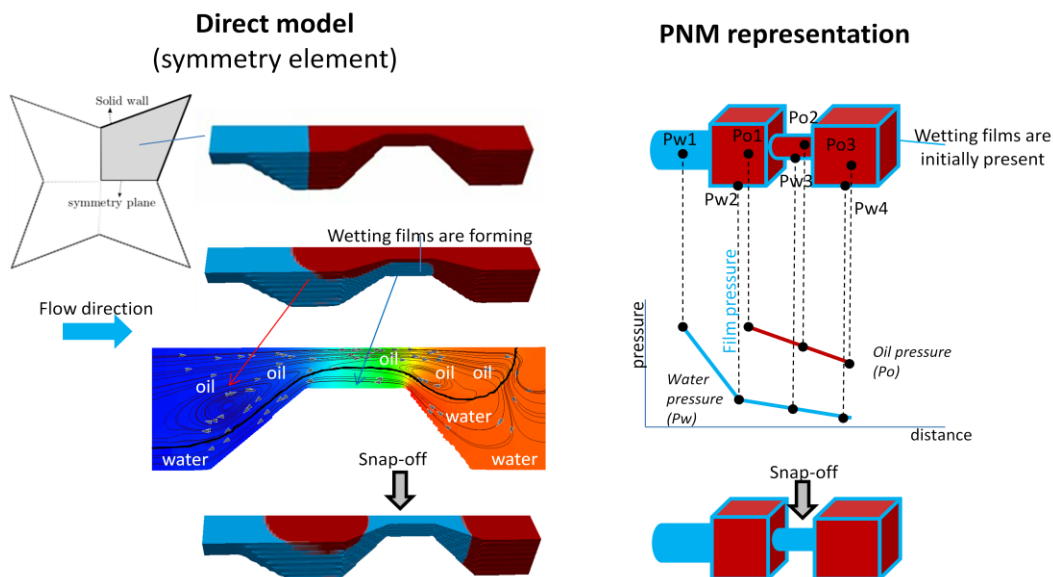


Figure 7: Imbibition modelled in a direct approach (showing only symmetry element, VoF method) [11] and the PNM representation. Red is oil (nonwetting), blue is water (wetting).

In order to model the snap-off events *ahead* of the interface (Figure 2a) the thin wetting films have to pre-exist everywhere. And solving Navier-Stokes, which involves second order spatial derivatives, the minimum number of grid blocks to represent a mobile phase is 4-5 for a no-slip boundary condition. At a resolution at  $10\ \mu\text{m}$ , for instance, the film would be around  $50\ \mu\text{m}$ . If we want to a film thickness of  $1\ \mu\text{m}$ , then for a 3D system we will require  $50^3$  times higher resolution. Subsequently, the computational cost will increase in cubic order. With PNM, on the other hand, introducing thin films does not introduce any additional cost; they “naturally” exist without any need for explicit gridding. Table 2 provides a benchmarking of the current PNM and direct method on simulation times for two-phase flow on similar physical size geometries.

Table 2. Information on resolution and runtimes of PNM and direct simulation [11].

Method	Physical size	Voxels	Throat /corner resolution	Pore resolution	Computer speed	Runtime
Direct	$1.33 \times 0.9 \times 0.9\ \text{mm}^3$	$230 \times 150 \times 150$	$5.549\ \mu\text{m}$	$11.1\ \mu\text{m}$	32 TFLOPS/s	3 days- medium Ca, 1 week- low Ca
PNM	$1 \times 1 \times 1\ \text{mm}^3$	$20 \times 20 \times 20$ elements	--	--	64 GFLOPS/s	0.5 day- medium Ca, 1 day- low Ca

The main advantage of direct models is that no extraction process is necessary; the flow can be solved directly on the images of the pore space. The uncertainties in the network geometry are irrelevant, therefore, has no implication on simulation results.

## APPLICATION TO ENHANCED OIL RECOVERY (EOR)

In improved and enhanced oil recovery, often chemical solutions or low salinity water are injected in order to alter the wettability or mobilize the oil. Often the associated transport processes are the rate-determining step. Molecular diffusion, for instance, is too slow as an effective transport mechanism. The wetting films, however, provide an effective means for transport of chemicals, e.g., ions, surfactant solution in chemical EOR. In this way, a wettability altering agent can flow ahead of the advancing meniscus via the thin films and alter the wettability to a more favourable condition.

Current PNM simulator is coupled to the geochemical software PHREEQC in order to simulate low salinity water injection. An example is displayed in Figure 8 which shows the occupancy in the network (left) and the salt ( $\text{CaCl}_2$ ) concentration (right) at the corresponding time. It clearly shows that the salt solution is distributed through the wetting films and reaches locations beyond the main displacement front. The salt is transported using the flow equation throughout the pore space and the adsorption is simulated using PHREEQC. A Langmuir isotherm is used. The contact angle and the interfacial tension is calculated locally based on the local concentration at each time step, and new  $P_c$  values are updated. The wettability altering agents in the injected solution modifies the wettability and hence the relative permeability and capillary pressure–saturation functions to more favorable conditions, which stabilizes the displacement.

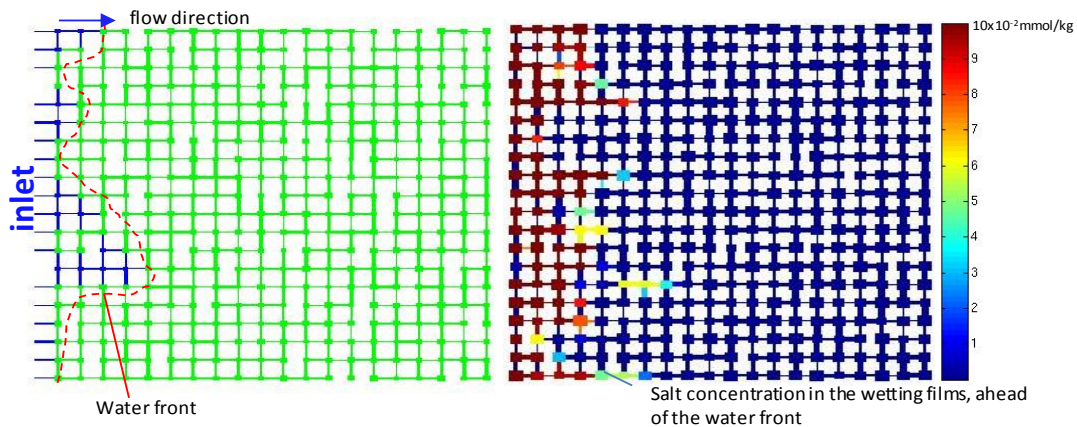


Figure 8: (a) oil (green)/water (blue) occupancy in a two-dimensional 20x20 network, (b) low salinity water flows through the wetting films (in the angular corners) ahead of the waterfront; salt concentration corresponding to case shown in (a). Initial  $\text{CaCl}_2$  concentration  $c_b = 0.01 \text{ mmol/kg}$ , injection rate  $i = 1\text{E-}16 \text{ m}^3 \text{ s}^{-1}$ ,  $\mu_{\text{oil}} = 1\text{E}^{-1} \text{ Pa.s}$ ,  $\mu_w = 1\text{E}^{-3} \text{ Pa.s}$ ,  $\sigma_{\text{ow}} = 0.03 \text{ N/m}$ .

This approach can be extended to model polymer adsorption, and various chemical EOR processes [12]. Diffusion and adsorption happen in molecular scale, significantly slower than advection. Therefore they are also the rate limiting processes; i.e. if the advection is too fast, then the diffusion and adsorption will never have chance to occur, instead the chemicals will be carried away in the flowing phase without affecting the wettability. In other words, the experiments and simulations have to be run under very low capillary numbers ( $Ca$ ). At such low rates the simulation times increase significantly for any method. With a grid based direct approach this is an extra burden additional to the cost of extra fine ( $nm$ ) gridding.

## CONCLUSIONS

Even though there is already progress in the physical representation of thin wetting films, many more challenges lie ahead. Improving experimental technologies will provide more direct access to the nano/micro scale physics and reveal more details. At the same time the workload on any petrophysics lab will constantly increase. The only way forward is to include the numerical techniques in the decision-making process wherever possible. In particular, when many runs are needed for a sensitivity analysis of various parameters (like in EOR), PNMs might be a more pragmatic choice given the current computational costs. This can be achievable only by further improvements, such as:

- Better physical thin film flow representation,
- Implementation of molecular processes, i.e. diffusion and adsorption,
- Implementation of processes during polymer injection, etc.

However any new development in physics would be reliable only if the extracted network is reliable. This is where the true challenge lies with PNMs.

## ACKNOWLEDGMENTS

Ali Raeini is acknowledged for providing the input for direct simulations.

## REFERENCES

- \* Corresponding author; E-mail address: evren.unsal@total.com
1. Lucia, F.J., “Rock-fabric/petrophysical classification of carbonate pore space for reservoir characterization”, *AAPG Bulletin*, (1995) **79**, 1275-1300.
  2. Anselmetti, F.S., S. Luthi, G.P. Eberli, “Quantitative characterization of carbonate pore systems by digital image analysis”, *AAPG Bulletin*, (1998) **82**, 1381-1405.
  3. Al-Kharusi, A.S., M.J. Blunt, “Network extraction from sandstone and carbonate pore space images”, *J Petro. Sci. Eng.*, (2007) **56**, 219-231.
  4. Szymkiewicz, A., “Upscaling from Darcy scale to field scale”, *Modelling Water Flow in Unsaturated Porous Media*, GeoPlanet, Heidelberg, (2013) 139-175.
  5. Tuller, M. and D. Or, “Hydraulic conductivity of variably saturated porous media: film and corner flow in angular pore space”, *WRR*, (2010) **37**, 1257-1276.
  6. Kim, E. and G.M. Whitesides, “Imbibition and Flow of Wetting Liquids in Noncircular Capillaries”, *J. Phys. Chem. B*, (1997) **101**, 855-863.
  7. Unsal, E., G. Mason, N.R. Morrow and D. Ruth, “Bubble snap-off and capillary back pressure during counter-current spontaneous imbibition into model pores”, *Langmuir*, (2009) **25**, 3387-3395.
  8. Joeker-Niasar, V., S.M Hassanizadeh, and H.K Dahle, “Non-equilibrium effects in capillarity and interfacial area in two-phase flow: dynamic pore-network modeling”, *J Fluid Mech.*, (2010) **655**, 38-71.
  9. Hammond, P., and E. Unsal, “A dynamic pore network model for oil displacement by wettability-altering surfactant solution”, *TIPM*, (2012) **92**, 789-817.
  10. Berg, S., H. Ott, S.A. Klapp, A. Schwing, R. Neiteler, N. Brussee, A. Makurat, L. Leu, F. Enzmann, O. Schwarz, M. Kersten, S. Irvine, and M. Stampanoni, “Real-time 3D imaging of Haines jumps in porous media flow”, *PNAS*, (2013) **110**, 3755–3759.
  11. Raeini, A.Q., M.J. Blunt and B. Bijeljic, “Modelling two-phase flow in porous media at the pore scale using the volume-of-fluid-method”, *J. Comp. Phys.*, (2012) **231**, 5653-5668.
  12. Unsal, E., P. Hammond, M. Schneider, “Effects of surfactant on wettability of oil recovery in a pore network model”, *16<sup>th</sup> European Symposium on Improved Oil Recovery*, Cambridge, UK, (2011), paper A09.